Check for updates

The growth behavior of brain-like SnO$_2$ microspheres under a solvothermal reaction with tetrahydrofuran as a solvent and their gas sensitivity

Yang Chen, Na Luo, Zhixin Li, Junping Dong,* Xiaohong Wang, [ID] Zhixuan Cheng and Jiaqiang Xu [ID] *

In this paper, the growth behavior of brain-like SnO$_2$ microspheres synthesized by a tetrahydrofuran (THF) solvothermal method was studied. Unlike water or ethanol as the solvent, THF is a medium polar and aprotic solvent. Compared with other common polar solvents, the THF has no strong irregular effects on the growth process of SnO$_2$. In addition, the viscosity of THF also helps the SnO$_2$ to form a regular microstructure. The growth behavior of the brain-like SnO$_2$ microspheres is controlled by changing the synthesis temperature of the reaction. The SEM and TEM results reveal that the SnO$_2$ forms particles first (125 °C/3 h), and then these nanoparticles connect to each other forming nanowires and microspheres (diameter ≈ 1–2 μm) at 135 °C for 3 h; finally the microspheres further aggregate to form double or multi-sphere structures at 180 °C for 3 h. In this paper, the brain-like SnO$_2$ microspheres obtained at 125 °C for 3 h were selected as sensitive materials to test their gas sensing performance at different operating temperature (50 °C and 350 °C). The H$_2$S was tested at 50 °C which is the lowest operating temperature for the sensor. The combustible gas (H$_2$/CH$_4$/CO) was measured at 350 °C which is the highest temperature for the sensor. They all have extremely high sensitivity, but only H$_2$S has excellent selectivity.

Introduction

Metal oxide semiconductor (MOS) materials are widely studied in many fields such as gas sensors,[1–5] lithium-ion batteries,[6–8] solar cells,[9–12] liquid crystal displays,[13,14] transparent conductive electrodes,[10,12] and so on.[15,16] SnO$_2$ has been studied in gas sensors, including the specific response research of combustible gas,[5,17] VOCs[4,18] and many other gases. Based on these different applications, a large number of SnO$_2$ with different morphology have been synthesized, including SnO$_2$ hollow nanospheres,[19–23] nanosheets,[24,25] nanosheet self-assembled spheres, SnO$_2$ thin film,[26,27] SnO$_2$ nanotubes,[17] SnO$_2$ nanowires[28] and so on. Most of them were synthesized by the hydrothermal method. However, the solvents of those synthesis reaction are generally deionized water or ethanol or water and ethanol. What's more, a certain kind of suitable material with target structure is always our purpose while ignoring the research on the chemical growth behavior of materials in the synthesis process, which should be the problem that chemical researchers should pay more attention to. Therefore, using other solvents instead of deionized water or ethanol to explore the growth behavior of SnO$_2$ is of great significance for the preparation of SnO$_2$ with new morphologies.

MOS gas sensors were born in Britain at the beginning of the 20th century, Because of their simplicity, efficiency, and wide application, people have not stopped the research of MOS gas sensor. Researchers have carried out extensive and in-depth research on the selectivity,[5,29,30] stability,[31,32] response,[33–35] and response time[36–38] of gas sensors. But most of the works reported are based on one operating temperature for a single or double gas-sensitive response. They did not consider the same material at different temperatures to realize the selectivity of gases. Furthermore, most of the reported work on a pristine SnO$_2$ still has certain shortcoming, such as high operating temperature and poor selectivity. Therefore, it is extremely important to explore SnO$_2$ sensors that have good selectivity at low temperatures. Moreover, exploring the response of the same material to different gases at different operating temperatures is meaningful, which cannot be ignored.

To observe the growth behavior of SnO$_2$ prepared by the solvothermal method, the medium polarity and aprotic THF was selected and used as a solvent to replace strong-polar solvent water who has strong irregular effects on its growth process. By controlling the temperature of this reaction, this conclusion was gotten: under the solvothermal condition of tetrahydrofuran, when the hydrothermal temperature is 125 °C, the synthesized brain-SnO$_2$ microspheres are assembled from nanoparticles. When the hydrothermal temperature rises to 135 °C, the structural units constituting the SnO$_2$ microspheres grow into nanowires or

NEST Lab, Department of Physics, Department of Chemistry, College of Sciences, Shanghai University, Shanghai 200444, PR China. E-mail: jpdong@shu.edu.cn; xujiaqiang@shu.edu.cn
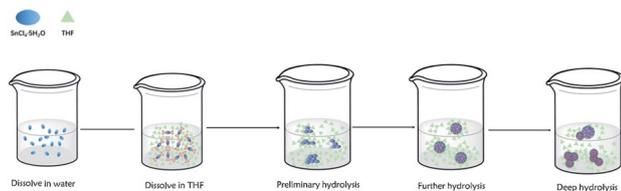
Scheme 1 Schematic diagram for the synthesis of SnO_2.

smaller microspheres (diameter $\approx$ 1–2 μm). When the hydrothermal temperature rises to 180 °C, the SnO_2 microspheres completely grow into a double or multi-sphere structure. The growth behavior of SnO_2 microsphere shows that the reaction temperature has a crucial influence on the growth of SnO_2. The brain-SnO_2 microspheres with good morphology were selected as sensitive materials to explore its response to H_2S gas at low operating temperature and H_2/CO/CH_4 combustible gases at high operating temperature. Finally, the results show that the brain-SnO_2 microspheres can realize the stable response to 0.1 ppm H_2S and no response for the rest of the common gases at 50 °C operating temperature. When the operating temperature is 350 °C, it can obtain the stable response to 1 ppm/H_2, 20 ppm/CH_4, and 80 ppm/CO, but it has poor selectivity under high temperature because of formaldehyde and H_2S have a great influence on those combustible gas. In fact, the interference of these two gases can be eliminated by whether the material has a response at low operating temperature, that is, the material has no response at low temperature, but has a response at high operating temperature, which is inevitably caused by combustible gas. By analogy, this elimination method can also be applied to other materials that have the same problem (Scheme 1).

Experiment

Medicines and instruments

Tetrahydrofuran (THF), 37% HCl, $SnCl_4 \cdot 5H_2O$, absolute ethyl alcohol, deionized water 100 ml hydrothermal kettle, blast oven, vacuum oven, ultrasonic instrument, MEMS gas-sensitive performance tester.

Synthetic procedure

2 g $SnCl_4 \cdot 5H_2O$ (A.R.) was dissolved into 80 ml tetrahydrofuran, and then the mixed solution was transferred into 100 ml hydrothermal kettle, which was kept in an oven at 125 °C, 135 °C, 150 °C and 180 °C for 30, 90 and 180 minutes respectively. The product was washed three times with deionized water and absolute ethyl alcohol, then the product was kept in a vacuum oven at 60 °C for 8 hours. Finally, the final product was prepared by calcined in a tube furnace at 350 °C for 2 hours.

Material characterization

DX-2700 powder diffractometer was adopted to conduct crystal powder diffraction analysis of the product from 5–90° under high pressure of 35 kV. The samples were analyzed by the Nova Nano SEM 450 field emission scanning electron microscope. The morphology of the samples was observed by the JEM-2100F field emission projection electron microscope.

Manufacture and performance test of gas sensor

The test of gas sensitivity is based on MEMS platform that is manufactured by our lab showed in Fig. 1 below. Fig. 1a is the schematic diagram of MEMS processing, Fig. 1b shows the MEMS that have been coated, coating, and uncoated, Fig. 1c is
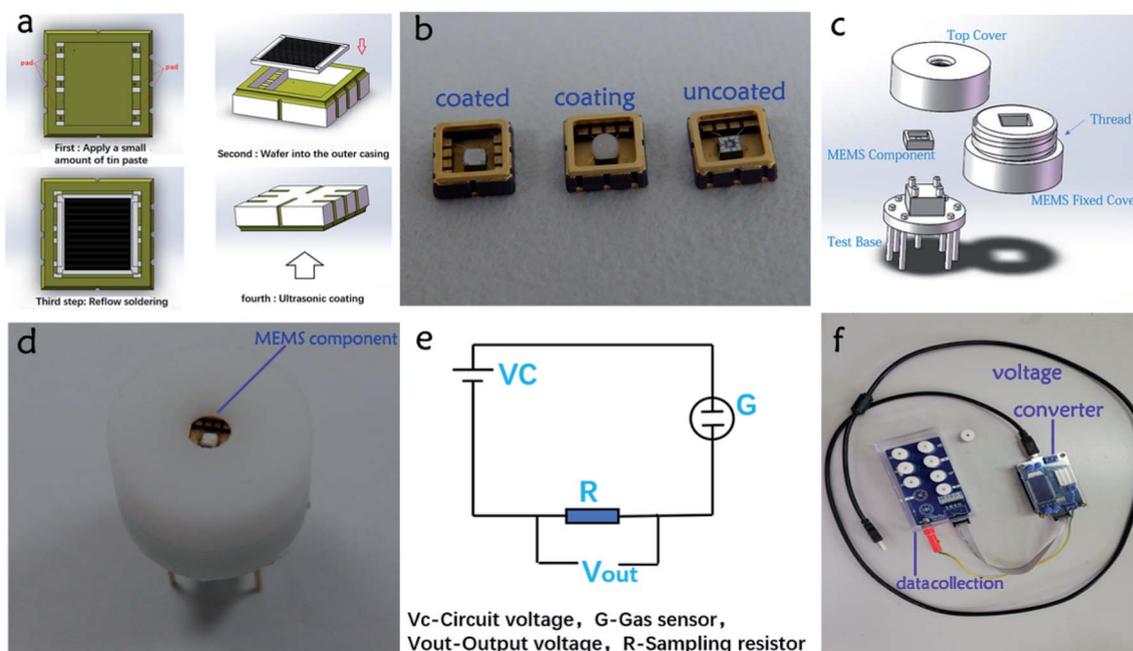

Fig. 1 (a) Processing of MEMS component; (b) coating materials on the MEMS; (c) the test base of MEMS gas sensor; (d) the entity of test base; (e) measuring circuit of MEMS gas sensor made by the author; (f) the test system of MEMS gas sensor made by our lab.
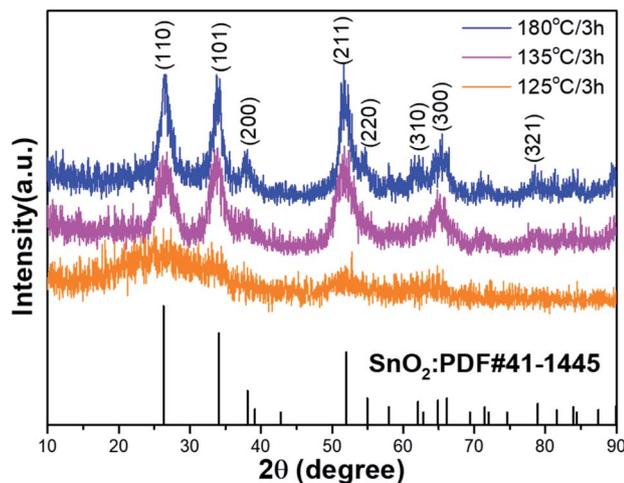
Fig. 2 X-ray diffraction patterns of SnO_2 to different reaction condition.

Fig. 3 FESEM image of SnO_2 to different reaction condition. (a and b) is the SnO_2 that get in 125 °C for 3 h; (c and d) is the SnO_2 that get in 135 °C for 3 h; (e and f) is the SnO_2 that get in 180 °C for 3 h.

the MEMS component test base, Fig. 1d is the entity of test base with MEMS components installed, Fig. 1e is the test circuit of MEMS gas sensor tester that made by the author, Fig. 1f is the entity of test system.

Characterization of the materials

Fig. 2 is the XRD pattern of the samples, it can be seen that all the products are rutile type SnO_2.[39,40] The product prepared at 125 °C/3 h only can see vaguely characteristic peaks, the characteristic peaks begin change to obvious as the reaction temperature goes up. As comparison with the graphs of 125 °C/3 h, 135 °C/3 h, and 180 °C/3 h, it is found that the higher the temperature is, the higher the crystallinity of SnO_2 is and the larger the particle diameter of the product is.

Fig. 3 is the morphology and structure characterization of samples by FESEM, Fig. 3a and b are the pictures of the samples obtained under the reaction conditions of 125 °C/3 h. The diameter of the microspheres is about 2 μm that can be seen from Fig. 3a, and its dispersion is good, and a small number of microspheres show a continuous growth trend of cross-linking with each other. Fig. 3b is a more detailed observation of the microstructure of a single microsphere. From Fig. 3b, it can be seen that this SnO_2 microsphere presents the surface structure of brain tissue, which is referred to the brain-SnO_2 microsphere in this paper. From the surface of this brain-SnO_2 microspheres, the evenly distributed tin oxide nanoparticles and nanowires can be seen, which proves that the growth process of this SnO_2 microsphere is to generate small SnO_2 nanoparticles first, and then the particles start to assembly with each other to form nanowires. As the growth progresses, the nanowires become longer and thicker, leading to the convergence of the strands, which can be observed in Fig. 3b. Fig. 3c and d are the SEM photos of samples obtained at 135 °C/3 h. By comparing the SnO_2 obtained at 125 °C/3 h, it can be seen that the surface of the SnO_2 microsphere (125 °C/3 h) is smooth, and there is no nanowire structure like that in surface of SnO_2 obtained at 125
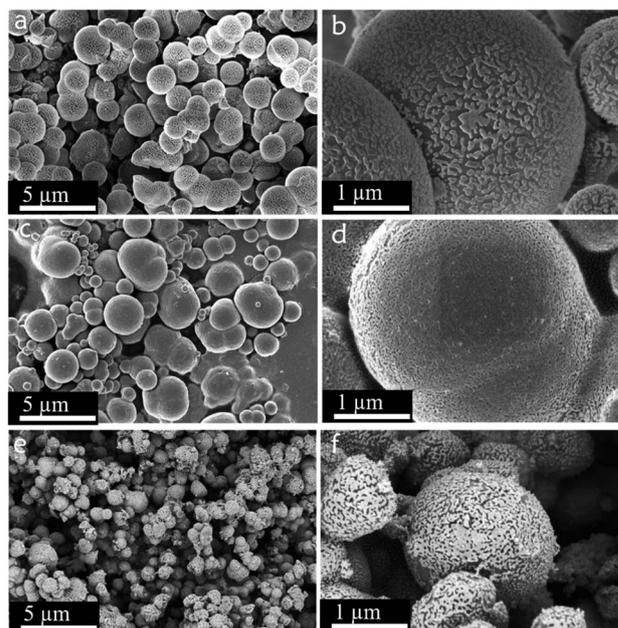
°C/3 h. However, the High magnification SEM spectrum reveals that the surface of the SnO_2 obtained at 135 °C/3 h is porous, which further proves that the nanowires will continue to crosslink and grow as the reaction temperature increases. Comparing Fig. 3c and a, it can be seen that there is also a joined together by two or more. From the above analysis, it can be concluded that the growth behavior of tin dioxide obtained by the hydrolyzed reaction of $SnCl_4 \cdot 5H_2O$ in THF is like this: the tin oxide particles formed first, then the nanoparticles connected into nanowires, under this circumstances, the nanoparticles and of the microspheres is about 1–2 μm. As the reaction progresses, the SnO_2 spheres begin to connect to form double or multi-sphere structures. Besides, samples at 180 °C/3 h were used for comparison, to illustrate that the reaction time and temperature have the same effect on its growth. As shown in Fig. 3e and f, this product was obtained at 180 °C/3 h, it can be seen that the morphology and structure of this product under this condition were similar to those who was prepared at 125 °C/3 h. The difference is that in the XRD pattern in Fig. 2, the peak pattern of 180 °C/3 h is clearer than that of 125 °C/3 h, which may be attributed to the denser internal structure of the microspheres.

To further prove the growth behavior of SnO_2 in THF. The SnO_2 microspheres obtained at 125 °C/3 h and 135 °C/3 h were ultrasonically treated for five minutes, and then the ultrasonically treated samples were characterized again by FESEM and FETEM, as shown in Fig. 4. Fig. 4a is the SEM photo of the sample at 125 °C/3 h, Fig. 4b is the TEM image of Fig. 4a that was ultrasonic treated after 5-minutes, and Fig. 4c is a part of Fig. 4b. By comparing Fig. 4a and b, it can be seen that this brain-SnO_2 microsphere was disintegrated after five minutes of ultrasound treatment. It breaks down into some wires and
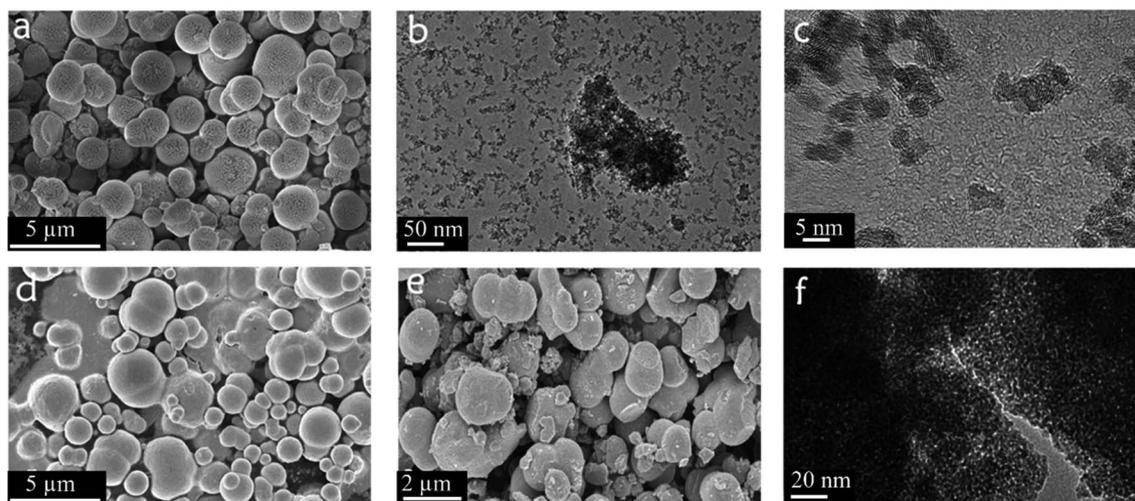
Fig. 4 (a) is the FESEM of SnO_2 get in 125 °C for 3 h, (b) is get from (a) that after ultrasonic treatment for five minutes, (c) is part of (b and d) is the FESEM of SnO_2 get in 135 °C for 3 h, (e) is get from d that after ultrasonic treatment for five minutes, (f) is the TEM of (e).

particles, Fig. 4c revealed that the diameter of the SnO_2 nanoparticles is about 5 nm. This confirms it again that the growth behavior is to form SnO_2 nanoparticles with a diameter of 5 nm first, and then the particles assemble into nanowires, finally, the nanoparticles and the nanowires form brain-SnO_2 microspheres. The Fig. 4d–f are the images of the sample that prepared at 135 °C/3 h. Different from the sample that prepared at 125 °C/3 h, the microspheres became unsmooth on the surface and exposed the solid structure but not been disintegrated. The Fig. 4f shows that there are many nanowires exist. Compared with the sample of 125 °C/3 h it can be seen that this sample was further reacted and the structure is harder and denser.

Materials	Detection concentration	OOP (°C)	Ref.
Cerebral-SnO_2	1 ppm-H_2	350	This paper
	20 ppm-CH_4		
	80 ppm-CO		
ZnO-QDS	1–4%/H_2	175	41
PtNPs on Au microchannels	>2.5%/H_2	—	42
Pd NP/SiO_2/Si	1%/H_2	27	43
Pt NP/WO_3	200 ppm/H_2	150	44
Pd island/SnO_2	250 ppm/H_2	300	45
ZnO nanorods	10 ppm/H_2	—	46
Pd-SWNT	6–100 ppm/CH_4	—	47
Ordered mesoporous In_2O_3	1300–6600 ppm/CH_4	350	48
ZnO	0.1–1%/CH_4	250	49
MoO_3	500 ppm/CH_4	500	50
TiO_2	400 ppm/CO	200	51
SnO_2/CuO	100 ppm/CO	180	52

Gas sensitive performance test

According to the above analysis, we select brain-SnO_2 microspheres obtained at 125 °C/3 h as a representative for further gas sensing test because it has a better spherical structure. Different from previous work, in this paper, the author selected two extreme operating temperatures to test various toxic and combustible gases. The test results show that at the operating temperature of 50 °C, the material only has a specific response to H_2S, and has no response to the rest of gases. In addition to its excellent selectivity, it has a good repeatable response to 1 ppm H_2S and is fully qualified for the international standard for the detection of H_2S that concentration in the air shall be not exceed 6 ppm. At the operating temperature of 350 °C, this kind of brain-SnO_2 microspheres can achieve a highly sensitive response to combustible gases, they are H_2, CO, and CH_4. Among them, it can achieve stable repeated detection of 1 ppm hydrogen, 20 ppm methane, and 80 ppm carbon monoxide, but at the 350 °C operating temperature, its selective performance has declined as a gas sensor material. That is, hydrogen sulfide and formaldehyde can achieve great interference to combustible gases. How to eliminate this interference? Maybe we can set a control group of low operating temperature. If there is no response at low operating temperature but have a response at the high operating temperature that there must be the response of combustible gases. As shown in Fig. 5, it is the test diagram of brain-SnO_2 microspheres for H_2S at the operating temperature of 50 °C. Fig. 5a is the material's test of a variety of common gases, they are 10 ppm H_2S, 10 ppm H_2, 100 ppm CO, 10 ppm C_2H_5OH, 10 ppm C_6H_6, 100 ppm CH_4, 10 ppm NH_3, 10 ppm HCHO, 10 ppm NO. From the Fig. 5a it can be seen that this material has excellent selectivity to H_2S at the operating temperature of 50 °C. It has no response to other gases and maybe this is because the operating temperature is too low for the other gases' chemically reactions. Fig. 5b is the original voltage data graph of the concentration gradient test, and the difference between the two adjacent gradients is 0.8 ppm. It can be seen from the figure that the change value of voltage keeps decreasing with the increase of fixed concentration. Fig. 5c is the test curve of H_2S at the concentration of 1, 2, 3, 4, 5 and
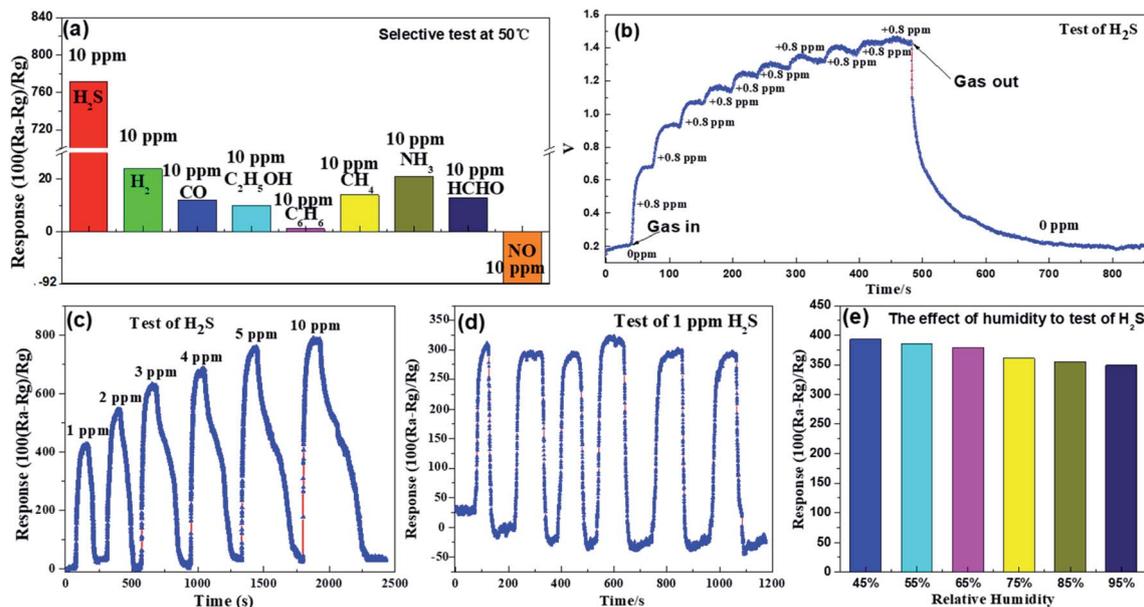
Fig. 5 Sensitivity test of material to hydrogen sulfide at 50 °C. (a) is the test of selectivity. (b) is the test of concentration gradient. (c) is the test of different concentration to H_2S. (d) is the test of 1 ppm H_2S. (e) is the effect of humidity on performance.

10 ppm. The response time is the 30 s, but the recovery time is relatively long, and it is prolonged with the increase of hydrogen sulfide concentration. Fig. 5d is a repeated stability test at 1 ppm H_2S, showing good consistency. Fig. 5e is the test of 1 ppm hydrogen sulfide under different humidity conditions. It can be seen that high humidity has a negative influence on

1 ppm H_2S detection, but the affected value is within the acceptable range.

In addition to achieving a highly sensitive response to hydrogen sulfide at a low temperature of 50 °C, the gas sensitivity of the material at a high operating temperature of 350 °C was also tested and found that the material has an excellent low
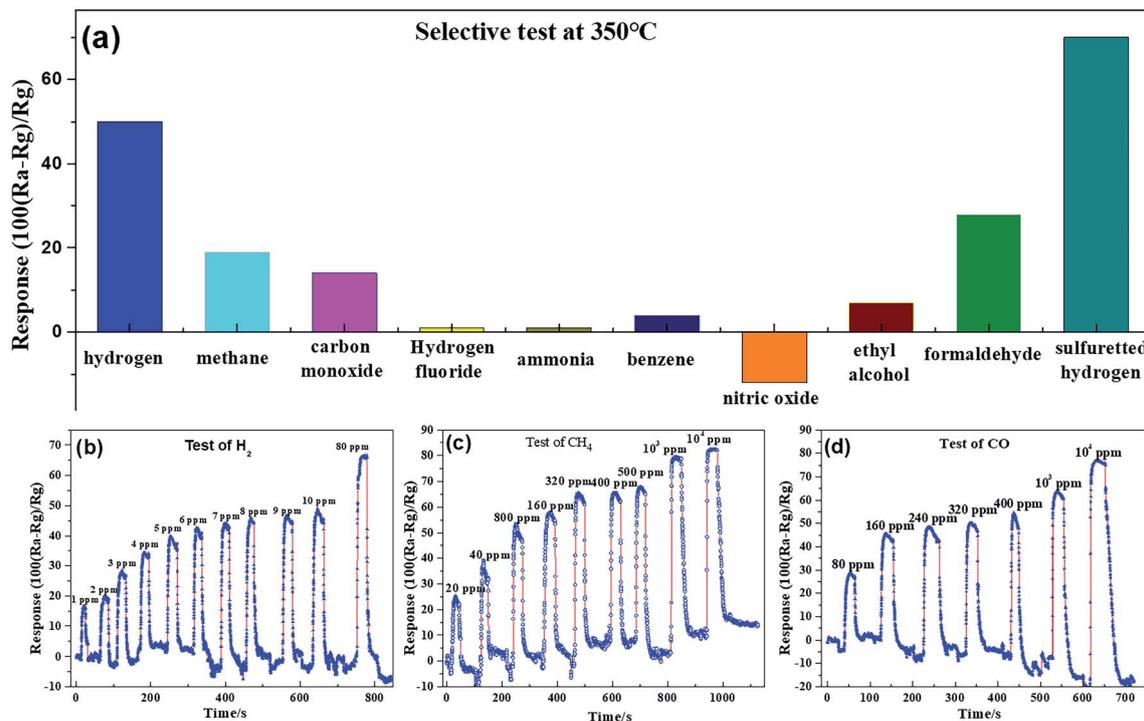

Fig. 6 Gas sensitivity test of combustible gas at 350 °C. (a) Is a selective test of the material for ten common gases. (b) Is the response of the material to H_2 (1–80 ppm). (c) Is the response of the material to methane (20–10 000 ppm). (d) Is the response to carbon monoxide (80–10 000 ppm).

concentration–response to $H_2/CO/CH_4$. As shown in Fig. 6a, is a selective test of the material for ten common gases. Compared with Fig. 5a, it can be seen that its selectivity has gotten significantly worse. Hydrogen sulfide and formaldehyde have great interference with its combustible gas response performance. Fig. 6c shows the response of the material to methane (20–10 000 ppm) at the operating temperature of 350 °C. It can be seen from this figure that the brain-SnO_2 microspheres have a high sensitivity to methane under a wide range of testing. Fig. 6d is the response to carbon monoxide at the operating temperature of 350 °C. It shows the response of 80–10000 ppm carbon monoxide. Besides, through literatures search, the performance table of gas-sensitive materials related to hydrogen/methane/carbon monoxide was sorted out. As shown in the table below, compared with the investigational work, the combustible gas sensor manufactured in this paper is at least one order of magnitude more sensitive than those. In the next work, we will continue to study the relationship between the gas sensing performance of SnO_2 and the hydrothermal temperature/time.

It is well known that the gas sensing properties of n-type MOSs rely on the change of surface chemisorbed oxygen when the sensor is exposed to air and target gas.[1,53] SnO_2 is a typical n-type semiconductor and its gas sensing mechanism can be explained by the remarkable resistance change when the sensor is exposed to air and tested gases.[4,54] When SnO_2 sensor in air atmosphere, oxygen molecules are adsorbed on the surface of SnO_2 to form chemisorbed oxygen (O^- and O^{2-}) by capturing electrons from SnO_2, resulting in the formation of an electron depletion layer (EDL) and the resistance is named R_a.[17] Upon SnO_2 sensor was exposed to H_2S gas, the chemisorbed oxygen ions O^- and O^{2-} will react with H_2S and electrons are released back to SnO_2 conduction band to recombine with holes, leading to a thinner EDL and a lower sensor resistance (R_g). Thus, the varied resistance in different atmospheres endows SnO_2 sensor with ability to sense H_2S.

Conclusion

In this paper, the growth behavior of SnO_2 synthesized in a solvent of tetrahydrofuran by the solvent-thermal method was studied. Its growth behavior is to generate nanoparticles (≈ 5 nm) first, then the nanoparticles are connected into nanowires, and the nanowires and nanoparticles are further self-assembled into microspheres. As the reaction proceeds, the microspheres are connected to each other to form multi-sphere structures. Besides, temperature and reaction time had the same effect on its growth behavior. The gas sensitivity of brain-SnO_2 microsphere prepared at 125 °C/3 h was tested, and it is found that the material had high sensitivity (0.1 ppm), excellent selectivity (only H_2S) and stability to H_2S at extremely low operating temperature (=50 °C). In this work, the author developed an ingenious and simple MEMS test platform, and the test is based on the MEMS component and MEMS test platform. It enriches the research and test methods of gas sensors with miniaturization and integration. Besides, considering that the operating temperature has a certain selectivity and sensitivity effect on the

gas sensitivity to sensing material, its gas-sensitivity at the extremely high operating temperature (350 °C) is also studied. It was found that the material had a good repeatable response to 1 ppm H_2, 20 ppm CH_4, and 80 ppm CO at this operating temperature, but its selectivity is poor. In the face of this problem, the author proposed a solution is to set a control group under low operating temperature conditions to determine whether the response under high operating temperature conditions is caused by combustible gases because at low operating temperature, the material has no response to combustible gas but has a response to interfering gas.

Conflicts of interest

There are no conflicts of interest to declare.

Acknowledgements

References

1 Y. Zhang, C. Wang, L. Zhao, F. Liu, X. Sun, X. Hu and G. Lu, *Sens. Actuators, B*, 2021, **341**, 130039.

2 L. Meng, W. Bu, Y. Li, Q. Qin, Z. Zhou, C. Hu, X. Chuai, C. Wang, P. Sun and G. Lu, *Sens. Actuators, B*, 2021, **342**, 130018.

3 Z. Kang, D. Zhang, T. Li, X. Liu and X. Song, *Sens. Actuators, B*, 2021, **345**, 130299.

4 K. Inyawilert, A. Sukee, M. Siriwalai, A. Wisitsoraat, J. Sukunta, A. Tuantranont, S. Phanichphant and C. Liewhiran, *Sens. Actuators, B*, 2021, **328**, 129022.

5 H. Bai, H. Guo, Y. Tan, J. Wang, Y. Dong, B. Liu, Z. Xie, F. Guo, D. Chen, R. Zhang and Y. Zheng, *Sens. Actuators, B*, 2021, **340**, 129924.

6 W. X. Zhang, H. Wang, P. Zhao and C. He, *Ionics*, 2021, **27**, 1–9.

7 Q. Tang, L. Wang, X. Ma and M. Li, *Mater. Lett.*, 2021, **294**, 129765.

8 Y. Shang, X. Liu, J. Zhang, C. Lu and C. Zhang, *Ionics*, 2021, **27**, 1967–1976.

9 C. Xu, Z. Liu, Q. Sun and E. C. Lee, *Sol. Energy*, 2021, **214**, 280–287.

10 J. J. Cao, K. L. Wang, C. Dong, X. M. Li and Z. K. Wang, *Org. Electron.*, 2021, **88**, 105972.

11 M. Abuhelaiqa, N. Shibayama, X. X. Gao, H. Kanda and M. K. Nazeeruddin, *ACS Appl. Mater. Interfaces*, 2021, **4**, 3424–3430.

12 H. Liu, Y. Li, J. Wu, Y. Fu, H. Tang, X. Yi and Z. Xie, *J. Mater. Chem. C*, 2021, **9**, 9914–9921.

13 N. M. Hadi and K. A. Ammar, *IOP Conf. Ser.: Mater. Sci. Eng.*, 2020, **928**, 072101.

14 J. Cui, X. Cao, F. Zhao, Z. Zhong and N. Han, *J. Asian Ceram. Soc.*, 2021, **1**, 1–14.

15 Y. Ma, L. Zhang, W. Shi, Y. Niu, B. Zhang and D. Su, *Chin. Chem. Lett.*, 2019, **30**, 183–186.

16 T. Gao, A. Kumar, Z. Shang, X. Duan, H. Wang, S. Wang, S. Ji, D. Yan, L. Luo, W. Liu and X. Sun, *Chin. Chem. Lett.*, 2019, **30**, 2274–2278.

17 X. Bai, H. Lv, Z. Liu, J. Chen, J. Wang, B. Sun, Y. Zhang, R. Wang and K. Shi, *J. Hazard. Mater.*, 2021, **416**, 125830.

18 J. H. Kim, P. Wu, H. W. Kim and S. S. Kim, *ACS Appl. Mater. Interfaces*, 2016, **8**, 7173–7183.

19 H. Xie, M. Chen and L. Wu, *Small*, 2017, **13**, 1604283.

20 B. Liu, Y. Li, L. Gao, F. Zhou and G. Duan, *J. Hazard. Mater.*, 2018, **358**, 355–365.

21 H. Cai, H. Liu, T. Ni, Y. Pan, Y. Zhao and Y. Zhu, *Front. Chem.*, 2019, **7**, 843.

22 C. H. Kwak, T. H. Kim, S. Y. Jeong, J. W. Yoon, J. S. Kim and J. H. Lee, *ACS Appl. Mater. Interfaces*, 2018, **10**, 18886–18894.

23 P. M. Bulemo, H. J. Cho, D. H. Kim and I. D. Kim, *ACS Appl. Mater. Interfaces*, 2018, **10**, 18183–18191.

24 G. Li, Z. Cheng, Q. Xiang, L. Yan, X. Wang and J. Xu, *Sens. Actuators, B*, 2019, **283**, 590–601.

25 D. Wang, L. Tian, H. Li, K. Wan, X. Yu, P. Wang, A. Chen, X. Wang and J. Yang, *ACS Appl. Mater. Interfaces*, 2019, **11**, 12808–12818.

26 I. H. Kadhim, H. A. Hassan and Q. N. Abdullah, *Nano-Micro Lett.*, 2016, **8**, 20–28.

27 N. Van Toan, C. M. Hung, N. D. Hoa, N. Van Duy, D. Thi Thanh Le, N. Thi Thu Hoa, N. N. Viet, P. H. Phuoc and N. Van Hieu, *J. Hazard. Mater.*, 2021, **412**, 125181–125193.

28 E. M. El-Maghraby, A. Qurashi and T. Yamazaki, *Ceram. Int.*, 2013, **39**, 8475–8480.

29 B. Zhang, Y. Li, N. Luo, X. Xu, G. Sun, Y. Wang and J. Cao, *Sens. Actuators, B*, 2020, **321**, 128461–128471.

30 H. Chen, X. Zhang, J. Zhang and Q. Wang, *Catal. Sci. Technol.*, 2018, **8**, 1126–1133.

31 H. Kim, Y. Pak, Y. Jeong, W. Kim, J. Kim and G. Y. Jung, *Sens. Actuators, B*, 2018, **25**, 460–468.

32 Y. Shi, Y. Zhu, B. Yu, Z. Gui, S. She, R. K. K. Yuen, H. Liu and Y. Hu, *RSC Adv.*, 2015, **5**, 41835–41838.

33 X. Li, Y. Li, G. Sun, B. Zhang, Y. Wang and Z. Zhang, *Sens. Actuators, B*, 2020, **304**, 127374–127384.

34 X. Dong, X. Cheng, X. Zhang, L. Sui, Y. Xu, S. Gao, H. Zhao and L. Huo, *Sens. Actuators, B*, 2018, **255**, 1308–1315.

35 H. S. Hong, N. H. Ha, D. D. Thinh, N. H. Nam, N. T. Huong, N. Thi Hue and T. V. Hoang, *Nano Energy*, 2021, **87**, 106165.

36 K. Hassan, A. S. M. I. Uddin and G.-S. Chung, *Sens. Actuators, B*, 2016, **234**, 435–445.

37 S.-W. Choi, A. Katoch, G.-J. Sun and S. S. Kim, *Sens. Actuators, B*, 2013, **181**, 446–453.

38 S. Zhang, T. Lei, D. Li, G. Zhang and C. Xie, *Sens. Actuators, B*, 2014, **202**, 964–970.

39 M. Yang, X. Zhang, C. Guo, X. Cheng, C. Zhu, Y. Xu, Z. Major and L. Huo, *Sens. Actuators, B*, 2021, **342**, 130067.

40 Y. Xu, J. Xie, Y. Zhang, F. Tian, C. Yang, W. Zheng, X. Liu, J. Zhang and N. Pinna, *J. Hazard. Mater.*, 2021, **411**, 125120.

41 R. Smrity, K. Chandan and K. Amit, *Nanotechnology*, 2019, **30**, 395501.

42 H. Ghulam, G. Mengchen and Z. Chuan, *Anal. Chim. Acta*, 2019, **1072**, 35–45.

43 G. B. Pour and L. F. Aval, *Results Phys.*, 2017, **7**, 1993–1999.

44 C. Zhang, A.-F. Kanta, H. Yin, A. Boudiba, J. D'Haen, M.-G. Olivier and M. Debliquy, *Int. J. Hydrogen Energy*, 2013, **38**, 2929–2935.

45 N. Van Toan, N. V. Chien, N. Van Duy, H. S. Hong, H. Nguyen, N. D. Hoa and N. Van Hieu, *J. Hazard. Mater.*, 2016, **301**, 433–442.

46 H. T. Wang, B. S. Kang and F. Ren, *Appl. Phys. Lett.*, 2005, **86**, 243503.

47 Y. Lu, J. Li, J. Han and H.-T. Ng, *Chem. Phys. Lett.*, 2004, **391**, 344–348.

48 T. waitz, T. wagner and T. sauerwald, *Adv. Funct. Mater.*, 2009, **19**, 653–661.

49 P. Bhattacharyya, P. K. Basu and H. Saha, *Sens. Actuators, B*, 2007, **124**, 62–67.

50 S. Barazzouk, R. P. Tandon and S. Hotchandani, *Sens. Actuators, B*, 2006, **119**, 691–694.

51 K. Hsu, T. Fang, Y. Hsiao and P. Wu, *J. Alloys Compd.*, 2019, **794**, 576–584.

52 A. Kumar, A. Sanger, A. Kumar and R. Chandra, *RSC Adv.*, 2016, **6**, 47178–47184.

53 J. Liu, L. Zhang, J. Fan, B. Zhu and J. Yu, *Sens. Actuators, B*, 2021, **331**, 129425.

54 P. H. Phuoc, N. N. Viet, L. V. Thong, C. M. Hung, N. D. Hoa, N. V. Duy, H. S. Hong and N. V. Hieu, *Sens. Actuators, B*, 2021, **334**, 129606.